# Practical limits for detection of ferromagnetism using highly sensitive magnetometry techniques

L M C Pereira, J P Araújo, M J van Bael, K Temst, A Vantomme

# Practical limits for detection of ferromagnetism using highly sensitive magnetometry techniques

**L M C Pereira[1,2,3], J P Araújo[1], M J Van Bael[4], K Temst[3], A Vantomme[3]**

[1] IFIMUP and IN-Institute of Nanoscience and Nanotechnology, Faculdade de Ciências da Universidade do Porto, 4169-007 Porto, Portugal
[2] Instituto Tecnológico e Nuclear, UFA, 2686-953 Sacavém, Portugal
[3] Instituut voor Kern- en Stralingsfysica and INPAC, K.U.Leuven, 3001 Leuven, Belgium
[4] Laboratory of Solid-State Physics and Magnetism and INPAC, K.U.Leuven, 3001 Leuven, Belgium

E-mail: `linomcp@fc.up.pt`

**Abstract.**

Over the last ten years, signatures of high temperature ferromagnetism have been found in thin films and nanoparticles of various materials which are non-ferromagnetic in bulk, from semiconductors to superconductors. These studies often involve state-of-the-art magnetometers working close to the limits of their sensitivity, where magnetic contaminations and measurement artefacts become non-negligible. Because such spurious effects may be involved, the reliability of magnetometry techniques for the detection of ferromagnetism in these new magnetic nanomaterials has been questioned. In this paper, we present a detailed study on magnetic contamination arising from sample processing and handling, describing how it may occur and how it can be avoided or otherwise removed. We demonstrate that, when proper procedures are followed, extrinsic magnetic signals can be reproducibly kept below $5 \times 10^{-7}$ emu ($5 \times 10^{-10}$ Am$^2$). We also give an overview of the expected levels of contamination when such optimum conditions can not be guaranteed and analyze the characteristics of the resulting magnetic behaviour, discussing which features may or may not be used as criteria to distinguish it from intrinsic ferromagnetism. Although the measurements were performed using superconducting quantum interference device (SQUID) magnetometers, most of what we describe can also be applied when using alternating-gradient force (AGFM) and vibrating-sample (VSM) magnetometers.

PACS numbers: 75.30.Cr, 75.75.-c, 75.50.Pp, 75.60.Ej, 07.55.Jg

Submitted to: *J. Phys. D: Appl. Phys.*

## 1. Introduction

Nano-objects with a magnetic signal comparable to that of the diamagnetic substrates on which they are deposited pose new challenges to state-of-the-art magnetometry and its users. With unrivaled sensitivity, superconducting quantum interference device (SQUID) magnetometers have long been proved suitable for the study of nano-versions of well understood materials, e.g., thin films or nanoparticles of magnetic materials and superconductors. However, when studying new materials exhibiting magnetic behaviour close to the limits of SQUID sensitivity, small magnetic contaminations and measurement artefacts must be carefully taken into account. This can be the case when studying, for example, dilute magnetic semiconductors (DMS), undoped oxides and superconductors, claimed to exhibit room temperature ferromagnetism (RT-FM) in thin-film or nanoparticle form. For many of these materials, RT-FM has been reported independently by various groups, the large majority based on SQUID magnetometry. However, an increasing number of reports suggest or even demonstrate that the observed ferromagnetism may originate from extrinsic sources, such as magnetic contamination [1, 2] or measurement artefacts [3].

Typically in these material systems, the already small signal of a small amount of (presumably) magnetic material is further decreased by the low concentration of magnetic dipoles and their small magnetic moment. To illustrate, let us consider a $5 \times 5$ mm$^2$ sample consisting of 10 monolayers of a material with a surface density of $1 \times 10^{15}$ atoms per cm$^2$ per monolayer from which 1% are dopant atoms or other magnetic point defects with a magnetic moment of 1 $\mu_B$. Such a sample, be it a continuous thin-film or nanostructures deposited on a diamagnetic substrate, has a total saturation moment of about $2 \times 10^{-7}$ emu (200 nemu) on a diamagnetic background. This can be thought of as the *nanomagnet* regime, where a nanoscale magnet (nm size) carries a nano-moment (nemu moment). However, this is also the regime where magnetic contamination and measurement artefacts become non-negligible. While some authors continue reporting on the ferromagnetic properties of these new nanomagnets solely based on SQUID measurements, the general opinion is moving towards the notion that finding a signature of ferromagnetism by means of SQUID magnetometry, i.e. a magnetic hysteresis, is only necessary but not sufficient to claim its existence [3].

Indeed, magnetometry by itself is insufficient to fully establish the magnetic nature of a given material, as it measures the total magnetic moment without any microscopic information. However, it provides in many cases information that other techniques hardly can assess. X-ray magnetic circular dichroism (XMCD) and polarized neutron reflectometry (PNR) suffer from limited detection power in dilute systems, in addition to the fact that they are only available at synchrotron and neutron facilities, respectively. Mössbauer and perturbed angular correlation (PAC) spectroscopies and other techniques based on hyperfine interactions are only applicable to a limited number of elements of the periodic table. Magneto-transport measurements may indirectly provide information about the magnetic character of a material system but require the input of models

which do not exist when the underlying magnetic mechanisms are unknown. In other words, SQUID magnetometry is to a large extent irreplaceable. However, in order to reproducibly establish its reliability limits when measuring very small magnetic moments, the sources of extrinsic magnetism should be investigated and either strategies to minimize them or criteria to identify them should to be outlined.

In this context, extrinsic magnetism can be distinguished between (i) setup-related artefacts leading to the misidentification of the magnetic state of a sample and (ii) magnetic contamination, i.e. magnetic material which is accidentally incorporated in the sample bulk or deposited on its surface and, therefore, is not accounted for in its nominal composition. A number of artefacts and limitations associated with SQUID magnetometers (i) have been identified in previous studies (e.g. [3, 4, 5, 6, 7]) as leading to various effects such as a small dependence of the measured magnetic moment on the sample size or shape or signal discontinuities due to automatic scale adjustment. All of these must be taken into account, in particular when high precision is desired. However, with one notable exception, none of these artefacts is capable of emulating ferromagnetism where it does not exist. The exception, recently identified and described in [3], consists of residual ferromagnetic-like hysteresis attributed to a small magnetic flux trapped in the superconducting coil. Also recently, various sources of magnetic contamination (ii) were identified [2]. The main conclusion from these studies is that artefacts inherent to SQUID magnetometers (i) can result in hysteresis with up to $4 \times 10^{-7}$ emu of saturation moment, whereas those associated with magnetic contamination (ii) due to sample handling or mounting can be as high as $1 \times 10^{-4}$ emu. Residual magnetic hysteresis and other artefacts constitute a technical limitation of the setup, and thereby set the lowest achievable limit for detection of ferromagnetism. If SQUID magnetometers are to be used as reliable tools to characterize nanomagnets, methods and procedures should be developed which ensure that the magnetic signal originating from contamination can be reproducibly kept below a well defined value, ideally of the same order or smaller than that from artefacts ($10^{-7}$ emu), in order to make full use of the setup sensitivity.

In this paper, we present a detailed study on magnetic contamination ($10^{-7}$ to $10^{-4}$ emu) arising from sample processing and handling. Purely diamagnetic substrates were used in order to isolate the magnetic contribution from the contaminant material. To ensure a statistically representative sample, we measured more than 50 pieces of commonly used substrates, $Al_2O_3$, Si, ZnO, MgO and $SrTiO_3$, of various thicknesses and suppliers, subject to various handling, processing and sample-mounting conditions. We investigated how contamination may occur and how it can be avoided or otherwise removed. We also analyzed the characteristics of the contaminant magnetism, discussing which features may or may not be used as criteria to distinguish it from intrinsic ferromagnetism. Although all the measurements were performed using superconducting quantum interference device (SQUID) magnetometers, most of what we describe can be applied when using alternating-gradient force (AGFM) and vibrating-sample (VSM) magnetometers.

## 2. Experimental details

The measurements were performed with the commonly used MPMS magnetometers from Quantum Design.‡ The majority was performed with an MPMS-XL (5 T) using the RSO option which provides higher sensitivity compared to the standard dc-transport mode. For comparison and completeness, some measurements were performed with a MPMS-5 (5.5 T), both in RSO and dc-transport modes. The samples consisted of approximately $5 \times 5$ mm$^2$ pieces of the commonly used substrates $Al_2O_3$, Si, ZnO, MgO and $SrTiO_3$, of various thicknesses ($t = 0.1 - 2$ mm) and suppliers (Crystal GmbH, CrysTec GmbH, MaTecK GmbH and SPC Goodwill Co. Ltd.). Given the large amount of samples, the measurements were simplified whenever possible. In most cases, the parameter to be determined was simply the saturation moment of the ferromagnetic component at 300 K, for which the *M-H* data were measured only for decreasing field (half-loops) and with a small number of field steps. Unless mentioned otherwise, all measurements were performed with the sample plane parallel to the applied field.

## 3. Results and Discussion

### *3.1. How contamination can occur*

#### *3.1.1. Sample mounting*

It is known that the sample mounting itself can contribute to a FM-like background, even if the sample is not contaminated [2]. As recommended by Quantum Design, clear plastic drinking straws are typically used as sample holders in SQUID magnetometers. Commercial cotton or Kapton® tape are commonly used to hold the sample inside the straw. Both Kapton® and cotton are diamagnetic materials. It is however known that the use of these materials can contribute to a FM-like background with a saturation moment of up to the order of $10^{-5}$ emu [2]. An alternative is to hold the sample simply by clamping it with the straw itself, avoiding the presence of additional material in the probed region. In principle, the deformations induced in the straw are minimal, behave linearly in field and are virtually temperature independent. However, special care must be taken when applying this method, as straw deformations have been reported to introduce a ferromagnetic-like background with a saturation magnetization of up to $1 \times 10^{-6}$ emu [2]. Furthermore, this *freestanding* method imposes some constraints on sample size and shape in order to ensure that the sample remains in place. A convenient alternative is to hold the sample with a polyester or cotton thread across the straw, tied around the sample, and held tight and straight by fixing it to the ends of the straw. This contributes with only a small amount of diamagnetic material around the sample, as the contribution from the remaining material cancels out due to its axial symmetry. If the material composing the thread is diamagnetic and free from ferromagnetic contaminations it does not contribute to any FM-like background

‡ Quantum Design, Inc., 11578 Sorrento Valley Road, San Diego, CA, USA.

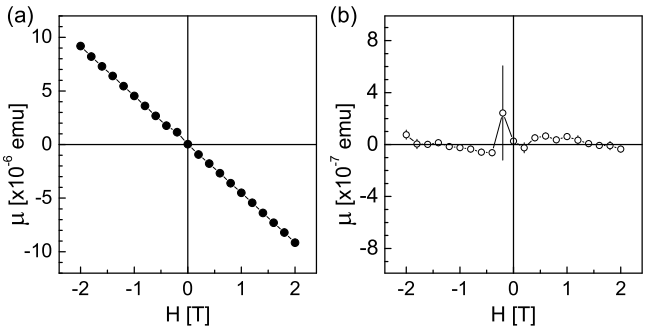


**Figure 1.** Example of *M-H* data at 300 K for typical thread-mounting, without any sample in order to isolate the background due to the thread (emu = $10^{-3}$ A m$^2$): (a) raw data measured between 2 T and -2 T; (b) after subtraction of the diamagnetic component determined by a linear fit to the raw data. The error bars correspond to the standard deviation of 5 consecutive measurements.

within SQUID sensitivity. Colored thread should be avoided as some of the commonly used pigments are magnetic. In any case, the materials that are used for sample mounting must always be tested, as they may be contaminated during production or handling in the laboratory. Figure 1 shows the 300 K *M-H* data (magnetic moment as a function of field) of such a thread-mounting scheme, without any sample, to isolate the contribution from the thread. The raw data (a) show an almost perfectly linear behaviour corresponding to a very small diamagnetic susceptibility. Subtracting this diamagnetic (linear) component results in a residual signal (b) with absolute value below $1 \times 10^{-7}$ emu, of the order of the system precision. Our tests revealed background levels consistently below $1 \times 10^{-7}$ emu. Unless mentioned otherwise, all the data that are shown in the following have been measured using this sample-mounting scheme.

### *3.1.2. Cleaving and handling*

The simplest and most obvious source of contamination is the contact with Fe-containing tools or setup parts. These can be the sample holder or clamps used during growth or post-growth treatments, tweezers and other tools used to manipulate a sample, or even non-Fe based tools or parts which have previously contacted magnetic materials. Among these, the most common source of contamination is probably the sample cleaving, even when a diamond stencil is used, since it is almost impossible to ensure that the rod, to which the diamond (or SiC piece) is attached, does not touch the sample. If the rod is composed of a ferromagnetic material, e.g., stainless-steel (SS), small magnetic particles can be deposited upon contact, depending on the hardness of the sample material and the pressure involved in the transfer process. Stronger contamination can occur, for example, when a sample is cleaved using a SS blade, a common alternative for substrates thicker than 0.5 mm. In this case, a much larger pressure is applied, as the blade is hammered onto the sample or substrate. The effect of cleaving on the magnetic response is illustrated in figure 2 (a) which shows the 300 K *M-H* half-loops of ZnO samples which have been cleaved using a Cu stencil (diamond

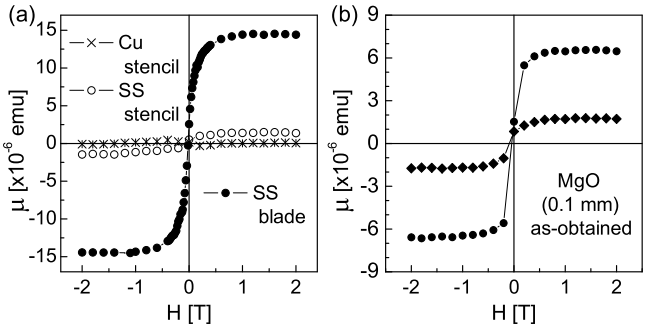


**Figure 2.** (a) 300 K *M-H* half-loops of ZnO (0.33 mm) samples which have been cleaved using a diamond-on-Cu stencil and a diamond-on-SS stencil and a $SrTiO_3$ (1 mm) sample cleaved with a SS blade. (b) 300 K *M-H* half-loops of pieces from two different MgO (0.1 mm) substrates, cleaved by simply pressing the very thin substrate while still inside the enclosing paper, as received from the supplier (emu = $10^{-3}$ A m$^2$).

on a Cu rod) or a SS stencil (diamond on a SS rod) and a thick $SrTiO_3$ sample ($t = 1$ mm) cleaved with a SS blade. The diamagnetic background was estimated by a linear fit between 1 T and 2 T and subtracted from the data. Cleaving ZnO with a Cu stencil did not introduce a measurable contamination. However, cleaving it with a SS stencil resulted in a FM-like signal with a saturation moment of $1.5 \times 10^{-6}$ emu. Cleaving $SrTiO_3$ with a SS blade resulted in an even stronger contamination ($1.4 \times 10^{-5}$ emu). Similar effects can be induced by contact with parts made of Ni- and Co-containing alloys, typically used in oxide-deposition setups.

Magnetic contamination can also occur when inks or silver paint are used for markings or for electrical contacts, respectively. These can contribute with a few $\mu$emu to a FM-like background [2] and should therefore be avoided prior to any magnetic characterization.

### *3.1.3. As-obtained substrates*

Surprisingly, some substrates may already be contaminated as received from the supplier. Figure 2 (b) shows the 300 K *M-H* half-loops of pieces from two different MgO (0.1 mm) substrates. The pieces were cleaved by simply pressing the very thin substrate while still inside the enclosing paper, as received from the supplier, thereby avoiding any contact with a possibly contaminating cutting tool. The saturation moment varies considerably among substrates between $10^{-6}$ and $10^{-5}$ emu. By measuring different pieces from the same substrate, we observed that the magnitude of the signal scales with the sample mass within 1%, irrespective of belonging to the border or to the interior of the substrate. This indicates that the contaminant material was uniformly distributed on the substrate surface, most likely during the polishing process. However rare, this shows the importance of a careful pre-characterization of the substrates.

### *3.1.4. High temperature processing / annealing*

In general, heating up a sample in contact with metallic parts results in material

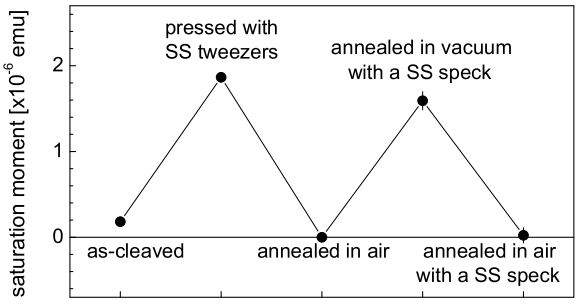


**Figure 3.** Saturation moment at 300 K of the same ZnO sample measured in four consecutive stages (emu = $10^{-3}$ A m$^2$): as-cleaved using a diamond-on-Cu stencil, pressed with a pair of SS tweezers, annealed at 900 °C in air for 10 min, annealed in vacuum under the same conditions but with a small SS speck on top and, finally, annealed in air once again.

transfer, even if the contact is point-like. In fact, material can even be evaporated from heated metallic parts and deposited on the sample without direct contact. This applies to high temperature film-growth as well as post-growth annealing. The particular physical and chemical reactions that take place depend on the materials involved and the temperature, atmosphere and duration of the process. Figure 3 shows the saturation moment measured at 300 K of the same ZnO sample in four consecutive stages of contamination and annealing. The non-magnetic ZnO sample becomes FM after being pressed with SS tweezers. The same occurs after annealing in vacuum at 900 °C for 10 min in contact with a small SS speck (few mg scraped from SS tweezers) placed on the sample surface before annealing and removed afterwards. For both types of contamination, annealing in air renders the sample again non-magnetic, most likely due to either oxidation or desorption of the contaminant material. We observed, although rarely, that annealing in *vacuum* can also reduce the contaminant magnetization, most likely due to desorption. These effects must be considered very carefully when studying, for example, the effect of annealing atmosphere on the magnetic properties of dilute magnetic semiconductors. Such reversibility phenomena can appear to provide evidence for the role of defects, introduced and removed by annealing in different atmospheres, in stabilizing the ferromagnetic state.

In order to minimize contamination, sample-holders made of non-metallic materials such as machinable ceramics should be used at all the steps of sample processing. However, this may be insufficient. Repeated use of the equipment can result in deposition of magnetic material in initially non-magnetic parts. For example, we have observed that, if the annealing setup is not properly cleaned and baked out, magnetic material with up to $5 \times 10^{-6}$ emu of saturation moment can be deposited on a sample during annealing even when it is performed in vacuum and using a ceramic sample holder.

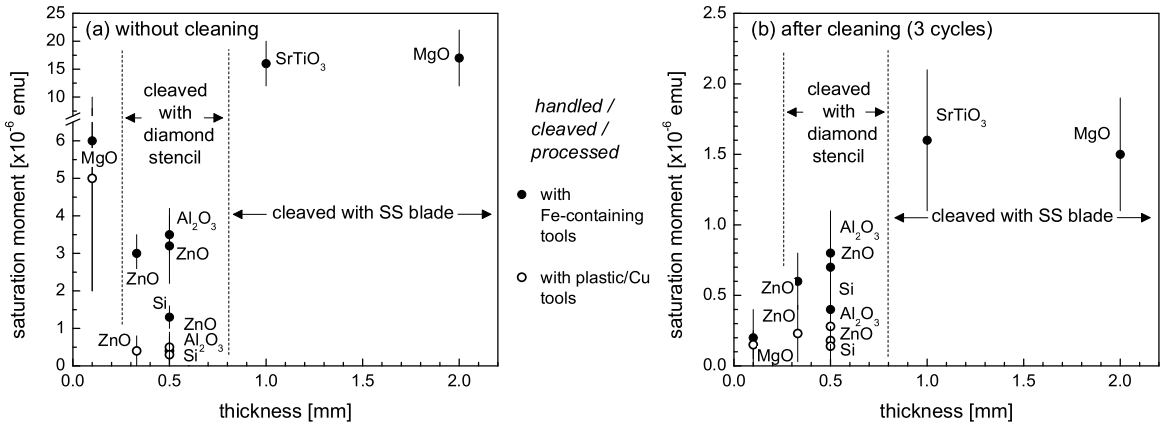


**Figure 4.** Summary of the average contamination levels for the different substrate materials and thicknesses before (a) and after (b) three cleaning cycles as described in the text (emu = $10^{-3}$ A m$^2$). Averages were taken separately for the samples for which Fe-containing tools were used in any of the processing steps. As indicated, thicker samples (1 and 2 mm) were cleaved using a SS blade, whereas the samples of intermediate thickness (0.33 and 0.5 mm) were cleaved using a diamond stencil (Cu/SS rod for Fe-containing/Fe-free tools). The thinnest MgO substrates (0.1 mm) were cleaved by simply pressing them with plastic tweezers while still inside the enclosing paper, as-received by the supplier. The effect of high temperature processing is not included. The error bars correspond to the standard deviation. Note that the maximum scale in panels (a) and (b) differs by one order of magnitude.

### *3.1.5. Accidental (re)contamination in metal-free conditions*

We have observed that even avoiding the contaminating conditions described above, some samples may accidentally become (re)contaminated. This is likely to originate from Fe-containing dust particles or other airborne magnetic debris easily found in laboratories where magnetic materials are synthesized or characterized. Such contaminant material can deposit on a sample directly or by transfer from otherwise non-magnetic tools or parts. Although the contribution from each of these random events is typically of the order of $10^{-6}$ emu, they can accumulate, depending on how many processing steps and how much exposure time precedes the magnetic characterization.

### *3.1.6. Summary*

Figure 4 (a) summarizes the different levels of contamination discussed above. In general, the oxides appear to suffer from higher contamination levels compared to Si, which reflects that metal particles are more easily abraded by harder materials. Whenever Fe-containing tools were used, the level of contamination reached an order of magnitude of $10^{-5}$ emu. On the other hand, they can be consistently kept below $1 \times 10^{-6}$ emu using only tools made of non-magnetic materials such as plastic, carbon fiber or copper. We note, however, that this corresponds to single-event contamination. For real samples, if the magnetic characterization is performed after several processing steps, the effects may accumulate. Moreover, the summary in figure 4 (a) does not

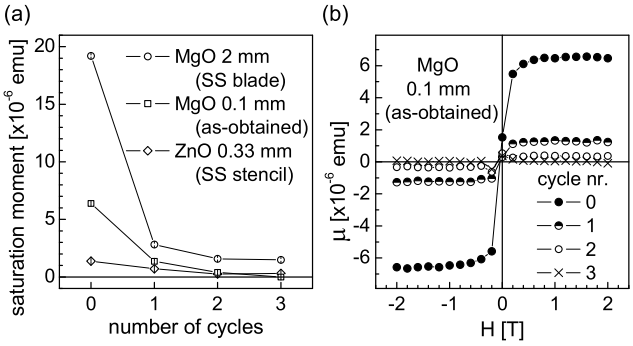


**Figure 5.** Representative examples of the effect of the cleaning procedure: (a) saturation moment (300 K) after each cleaning cycle of an MgO (2 mm) sample cleaved using a SS blade, an MgO (0.1 mm) sample contaminated as received by the supplier and a ZnO (0.33 mm) sample cleaved using a diamond-on-SS stencil; (b) 300 K *M-H* half-loops of the MgO (0.1 mm) sample (emu = $10^{-3}$ A m$^2$). Each cycle consists of three consecutive ultrasound baths in acetone, 2-propanol and ultrapure water, 5 min each.

include the effect of high temperature processing, which by itself can contribute with signals of the order of $10^{-6}$ emu.

### *3.2. How the contaminant material can be removed*

So far we demonstrated that the magnetic signal originating from contaminant material can be consistently kept below $1 \times 10^{-6}$ emu when proper procedures are followed. Nonetheless, real samples may suffer from multiple contamination events and accumulate larger magnetic signals, and in some cases, potentially contaminating conditions simply can not be avoided, e.g., when the substrates are already contaminated as received. In such cases, a suitable cleaning procedure is required for the removal of the contaminant material. Although acid cleaning procedures are standard for Si processing, most of the materials under consideration in this work (oxides) can be degraded by acids. Alternatively, we observed that cleaning the samples in consecutive ultrasound baths of acetone, 2-propanol and ultrapure water, for 5 min each, reduces the contamination considerably. In most cases, repeating this cycle for a number of times reduces it even further. We observed that the magnetic signal originating from the contaminant material reaches a minimum and saturates typically after three cycles. This is illustrated in figure 5 (a) where the saturation moment at 300 K is shown for various representative examples after consecutive cleaning cycles: a ZnO sample cleaved with a diamond-on-SS stencil, an MgO (0.1 mm) sample contaminated as received and an MgO (2 mm) sample cleaved with a SS blade. Figure 5 (b) shows the 300 K *M-H* half-loops of the MgO (0.1 mm) sample after each cleaning cycle.

Typically, the cleaning is very efficient when the pressure involved in the process of material transfer is small, as when scratching the back of a substrate with a diamond stencil. However, when the pressure is large enough, e.g., when cleaving a sample by hammering it with a SS blade, or when the contaminated sample has been subject to

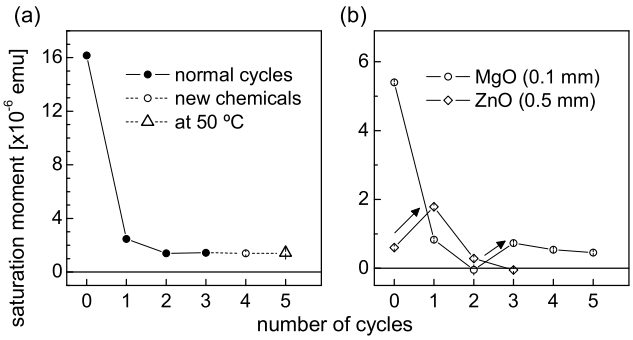


**Figure 6.** Saturation moment after each cleaning cycle for two non-typical cases (emu = $10^{-3}$ A m$^2$): (a) attempts to eliminate persistent contamination on an MgO (2 mm) substrate (cleaved with a SS blade) using new chemicals (○) and carrying out the baths at 50 °C (△); (b) MgO and ZnO samples accidentally recontaminated between cleaning cycles (↗). Note that the error bars are included (although too small to be visible), taking into account the experimental error and reproducibility limits (of the order of $10^{-7}$ emu).

high temperatures, the contaminating material may not be completely removed. In these cases, as shown in figure 6 (a), the strong adhesion with the sample prevents the complete removal of the contaminant material even when new chemicals (to prevent saturation) and higher temperatures (to increase the cleaning efficiency) are used. Moreover, our experience indicates that many short cycles are more efficient than a few long ones, e.g., three 5 min cycles instead of one of 15 min.

As described above, some of the studied samples were accidentally contaminated even in controlled conditions. Figure 6 (b) shows two of these cases. The increase in saturation moment indicates that these samples were contaminated between the end of the corresponding cleaning cycle and the start of the measurement, despite the efforts to avoid contaminating conditions. Interestingly, the nature of the contamination seems to differ from one case to the other. In only one of them, the contaminant material can be removed completely by cleaning.

Figure 4 (b) gives an overview of the persistent-contamination levels that are achievable with the described cleaning procedure. For the samples that had been in contact with Fe-containing materials, these are of the order of $10^{-6}$ emu. Remarkably, contamination levels below $5 \times 10^{-7}$ emu can be consistently achieved after cleaning if the samples have not contacted Fe-containing materials.

The applicability of such cleaning procedures is a trade-off between the required sensitivity for a given experiment and possible undesired effects of the cleaning. The ultrasound bath may damage the sample if it consists, for example, of nanostructures deposited on a substrate with poor adhesion. Also, H diffusion into the sample may be promoted or accelerated by the immersion in water, acetone or 2-propanol, and modify the sample's electrical and magnetic properties. By means of hydrogen forward scattering spectrometry (HFS), we investigated the hydrogenation effects of a 3-cycle cleaning sequence on the different materials used in this study (data not shown). We

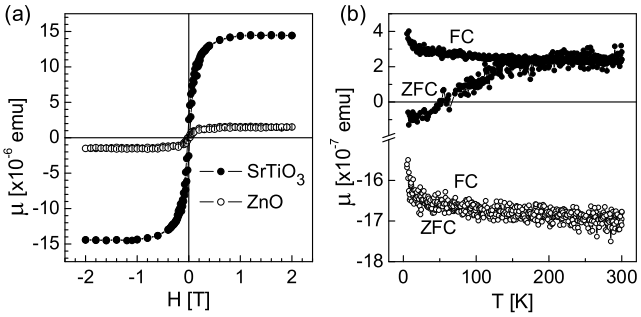


**Figure 7.** *M-H* and *M-T* data of a $SrTiO_3$ sample cleaved with a SS blade and a ZnO sample pressed with SS tweezers: (a) 300 K *M-H* full loops (2 T → -2 T → 2T); (b) field-cooled (FC) and zero-field-cooled (ZFC) measurements, with a field of 10 mT (100 Oe) as described in the text (emu = $10^{-3}$ A m$^2$). Unlike the *M-H* data (a), the *M-T* data (b) have not been corrected from the diamagnetic component.

found that the cleaning procedure does not introduce measurable amounts of H within the HFS sensitivity (< 1%). We note, however, that this is the case for the high-quality single-crystalline materials that we have studied. In real samples, such as thin films and nanostructures deposited onto these substrates, with possibly lower crystalline quality and therefore lower diffusion barriers, hydrogenation may occur.

### *3.3. How to distinguish contaminant from intrinsic ferromagnetism*

We have shown that a measurable magnetic contamination will most likely occur if proper procedures are not followed. In general, cleaning procedures can be applied, but in some cases they are unable to completely remove the contaminant material. In other cases, cleaning may not even be an option if it affects the intrinsic properties of the samples. Next, we analyze the magnetic behaviour of the contaminant material, discussing which features may or may not be used as criteria to distinguish it from intrinsic ferromagnetism in these cases where it can not be excluded that measurable contamination has occurred.

#### *3.3.1. General M-H and M-T behaviour*

Figure 7 shows the typical *M-H* and *M-T* behaviour of two contaminated samples with saturation moment in the $10^{-6}$ to $10^{-5}$ emu range. In general, both for weakly and strongly contaminated samples, the *M-H* curves show a coercivity of 10 – 100 mT (100 – 1000 Oe) and a remanence of 10% – 20% of the saturation moment. The field-cooled (FC) and zero-field-cooled (ZFC) measurements§ of the sample with higher

§ The following procedure was adopted for the field-cooled (FC) and zero-field-cooled (ZFC) measurements. The samples were demagnetized at 300 K and cooled without an applied magnetic field. After stabilizing the temperature at 5 K, a field of 10 mT (100 Oe) was applied. The magnetic moment was then measured as a function of increasing temperature from 5 K to 300 K - the zero-field-cooled (ZFC) measurement. The sample was then cooled in the same magnetic field and, after stabilizing at 5 K, the magnetic moment was measured again as a function of increasing temperature

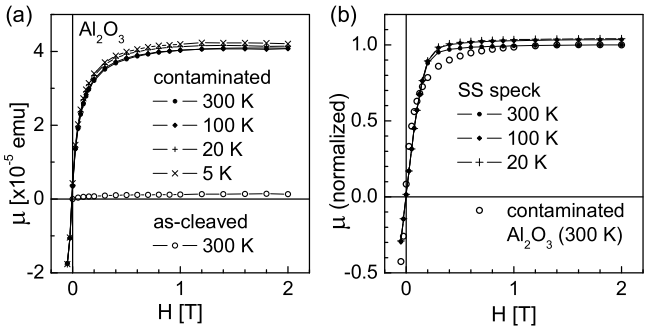


**Figure 8.** Comparison between *M-H* data for positive decreasing field at various temperatures: (a) $Al_2O_3$ sample before (at 300 K) and after (at 5, 20, 100 and 300 K) being contaminated by SS tweezers; (b) 300 K *M-H* data of the contaminated $Al_2O_3$ sample compared to the 20 K, 100 K and 300 K *M-H* data of a small speck of the SS tweezers tip that caused the contamination (emu = $10^{-3}$ A m$^2$).

saturation magnetization ($SrTiO_3$) show some degree of irreversibility which disapears well below the Curie temperature ($T_C > 300K$). This is consistent with a scenario of superparamagnetic (SPM) behaviour of the metallic particles abraded from the SS blade. The ZnO sample does not show FC-ZFC irreversibility, which could be interpreted as a sign of a fundamentally different type of magnetic behaviour from that of the $SrTiO_3$ sample. We note, however, that the saturation moment of the ZnO sample is much smaller to start with [Fig. 7 (a)], i.e., the SPM component and consequently the expected FC-ZFC splitting are much smaller. Assuming the same linear correspondence between the saturation moment and the FC-ZFC splitting for both samples, the maximum FC-ZFC splitting expected for the ZnO sample is of about $5 \times 10^{-8}$ emu, smaller than the experimental noise. Therefore, even though the ZnO sample shows measurable coercivity and remanence up to 300 K, FC-ZFC irreversibility is not observed because the possible splitting can not be resolved. We also note that the *M-T* data in Fig. 7 (b) have not been corrected from the diamagnetic component, which results in a shift of the data towards negative $\mu$. This explains why the ZnO moment is negative and the $SrTiO_3$ ZFC curve crosses zero around 50 K. Because the diamagnetic susceptibility is larger for ZnO compared to $SrTiO_3$, this also explains the large off-set between the data for the two materials.

Figure 8 (a) shows the *M-H* data at different temperatures of an $Al_2O_3$ sample that has been intentionally contaminated using SS tweezers. Aside from a small increase in saturation moment with decreasing temperature (3% between 300 K and 5 K), characteristic of ferromagnetic materials with a Curie temperature well above 300 K, the measured $\mu(H)$ is virtually temperature independent. For conventional SPM behaviour, $\mu(H)$ is given by a Brillouin function (Langevin in the continuous limit) which is a function of $H/T$. Therefore, for SPM behaviour, the saturation field at 300 K is expected to be about 60 times that at 5 K. This is clearly not the case;

from 5 K to 300 K - the field-cooled (FC) measurement.

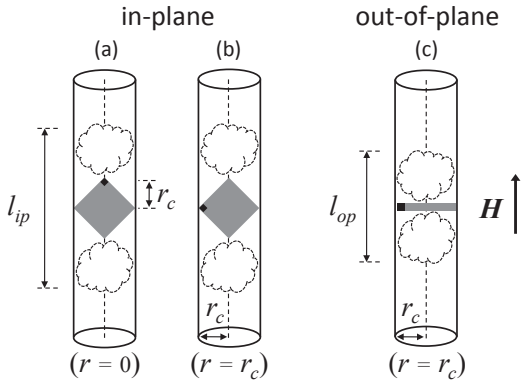


**Figure 9.** Diagram illustrating possible sources of *radial* and *axial* anisotropy artefacts for in-plane [(a) and (b)] and out-of-plane (c) measurements, as described in the text. The cylinders represent measuring straws and the samples are depicted in gray. *Radial effects* can be created by the contaminant material (depicted as black squares on the samples edges) at a distance $r_c$ from the sample center and $r$ from the measuring axis (vertical). *Axial effects* can be created, for example, when contaminated cotton is used to hold the sample (depicted above and below the samples), resulting in apparently different sample sizes ($l_{ip}$ and $l_{op}$).

the observed saturation behaviour is the same. This indicates that the contaminant-particle size is above the single-domain regime, i.e., the Brillouin/Langevin behavior of single-domain (macro-spin) SPM particles does not hold. In figure 8 (b), the 300 K *M-H* data of the contaminated $Al_2O_3$ sample are compared to the 20, 100 and 300 K *M-H* data of a small speck of the SS tweezers tip that caused the contamination. The same temperature independence is observed. However, the saturation behaviour differs considerably between bulk and abraded material. This indicates that not only the nature of the contaminant material but also the size and shape of the abraded particles determines its magnetic properties.

In summary, the magnetic behaviour of the contaminant material ranges from SPM-like to weak ferromagnetism. It is generally characterized by a small coercivity and remanence, saturation fields of the order of 1 T and FC-ZFC splitting which may however be too small to be resolved. In some cases, most likely when the Curie temperature of the contaminant material is far beyond the measured range and the contaminant-particle size is above the single-domain regime, the ferromagnetic component of the *M-H* loops is virtually temperature independent. Unfortunately, rather than distinctive, these characteristics are in fact typical of the new magnetic nanomaterials mentioned in the introduction.

*3.3.2. In-plane vs. out-of-plane anisotropy*

Diamagnetism is an isotropic property. Superparamagnetic or ferromagnetic contaminant particles may display some degree of single-particle anisotropy but since they are randomly placed in a sample, their net magnetization should also be isotropic. Therefore, a diamagnetic substrate, even if contaminated with FM material, is not

expected to show anisotropic magnetization with respect to the field direction. As such, anisotropy effects could in principle be used as a distinctive feature of intrinsic ferromagnetism. However, as we discuss next, the finite sample size or a non-uniform distribution of the contaminant material can lead to an apparent anisotropy when comparing measurements performed with the field parallel (in-plane) and normal (out-of plane) to the sample surface.

Similar to other extraction techniques, SQUID magnetometers rely on the response of pickup coils to changes in the magnetic flux as the sample is scanned through the coils. The response depends not only on the magnitude of the sample magnetic moment, i.e., of the ensemble of point dipoles, but also on their orientation and position with respect to the pickup coils. For non-spherical samples this automatically results in an apparent in-plane *vs.* out-of-plane anisotropy, even in the ideal case for which the diamagnetic and ferromagnetic components are uniformly distributed in the sample volume. For typical sample geometries, approximately $5 \times 5 \times 1$ mm$^3$, the measured magnetization is apparently larger by 3-4% in out-of-plane measurements, as demonstrated theoretically and experimentally in [7] and [3], respectively. This affects both diamagnetic and ferromagnetic components, and thus emulates a small magnetic anisotropy. Stronger anisotropy effects are created by non-ideal conditions, such as spatial asymmetries or non-uniformities of the ferromagnetic volume. Due to the cylindrical symmetry of the axial second-order gradiometers commonly used in SQUID magnetometers, these anisotropy artefacts can be divided into radial and axial effects.

*Radial effects* are observed when the radial distribution of the ferromagnetic volume is significantly different for different measurement geometries. To illustrate, let us consider a square diamagnetic sample, centered within the pickup coils, with a point-like contamination in one of its edges at a distance $r_B$ from the sample center (figure 9). By rotating the sample around its center, one can vary the radial distance $r$, of the ferromagnetic contamination relative to the longitudinal axis of the coils, between 0 and $r_c$ [figure 9 (a) and (c)]. Since the magnetic flux across the coils increases with $r$ (cf. [2]), so does the measured moment. As such, in-plane measurements may yield a smaller magnetization if the sample is oriented so that $r = 0$ [figure 9 (a)], whereas for out-of-plane measurements, $r = r_c$ always [figure 9 (c)]. These radial effects have been discussed in [2], where a ferromagnetic component up to 40% larger when measuring out-of-plane has been reported. We note, however, that we have not observed a radial anisotropy larger than 10%. We also note that radial effects may as well result in purely in-plane anisotropy, since in-plane rotation around the sample center can also vary $r$ between 0 and $r_c$ [figure 9 (a) and (b)].

*Axial effects* are controlled by the longitudinal elongation of the magnetic volume. The response of a point dipole with magnetic moment $\mu$, at point $z$ on the measurement axis and aligned with it, is given by

$$V(z) = \mu S\{2(r_c^2 + z^2)^{-3/2} - [r_c^2 + (z + \Lambda)^2]^{-3/2}$$

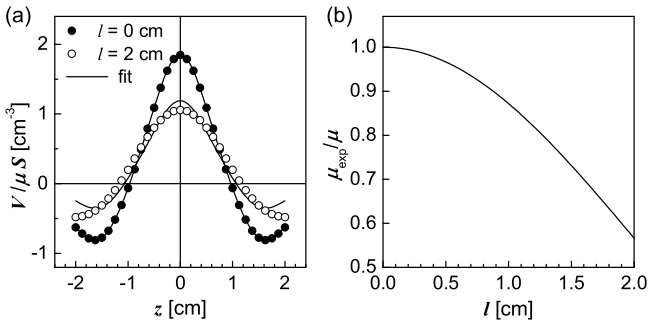


**Figure 10.** (a) Response curves ($V(z)$) for scans of two samples with equal magnetic moment $\mu$ and different geometries, simulated (∘ and •) using the finite elements calculation described in the text and best fits (line) of equation (1) using an algorithm similar to that used by the MPMS MultiVu application to deduce the measured moment $\mu_{\rm exp}$: a point-like dipole (•) and a line-like sample with length $l = 2$ cm along the gradiometer axis (∘). (b) Fitted $\mu_{\rm exp}$ as a function of sample length $l$.

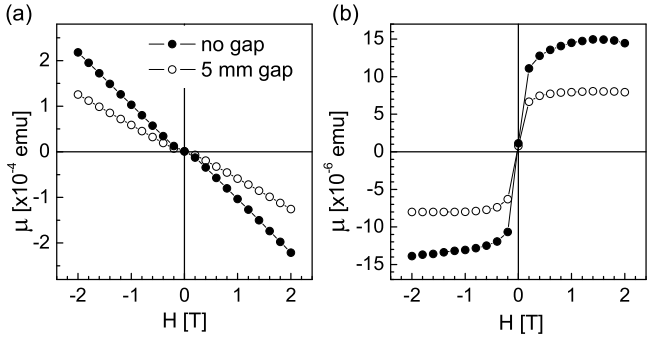


**Figure 11.** M-H half-loops of two small cotton pieces inside a measuring straw with no gap (•) and with a 5 mm gap (∘) between them: (a) raw data; (b) data corrected from the diamagnetic component estimated between 1 and 2 T (emu = $10^{-3}$ A m$^2$).

$$-[r_c^2 + (z - \Lambda)^2]^{-3/2}\}, \tag{1}$$

where $r_c$ is the coil radius (0.97 cm), $\Lambda$ is the distance between an outermost coil and the central coils of the gradiometer (1.519 cm) and $S$ is the calibration factor. Finite size samples with length $l$ along the $z$-axis can be approximated as an ensemble of point dipoles along the sample length $l$, neglecting the radial dimension. The $V(z)$ scans can thus be simulated using a simple finite elements calculation and fitted to equation (1) using an algorithm similar to that used by the MPMS MultiVu application to deduce the measured moment $\mu_{\rm exp}$. This is shown in figure 10 (a) for two limiting cases with equal moment $\mu$: a point-like dipole and a line-like sample with $l = 2$ cm. Figure 10 (b) shows how $\mu_{\rm exp}$ decreases with increasing sample length $l$. Within normal sample sizes ($\leq 0.5$ mm) the effect is negligible ($\leq 4\%$). However if the ferromagnetic signal is external to the sample, the effects may become significant. As mentioned above, in order to fix the position and orientation of a sample inside the measuring straw, it is common to use two small pieces of commercial cotton, which is typically contaminated with small ferromagnetic particles. If the sample is fixed between two pieces of cotton (figure 9),

the distance between the two pieces is very small (of the order of the sample thickess) for out-of-plane measurements, whereas for in-plane measurements, it is increased to about the sample length. In terms of *apparent* sample length, this corresponds to an increase from $l_{op}$ to $l_{ip}$ (figure 9). Figure 11 shows the *M-H* half-loops of two small cotton pieces inside a measuring straw, emulating the two measurement geometries: touching (in-plane) and separated by 5 mm (out-of-plane). The anisotropy is close to 100% and affects equally the diamagnetic and ferromagnetic components.

*3.3.3. N-shaped $V(z)$ and kinks in $\mu(H)$*

None of what we described so far can be used as a distinctive feature of contaminant magnetism. The search for such a fingerprint must therefore be extended to what is *experimentally* characteristic of measuring a contaminated sample, other than the magnetic behaviour itself. Indeed, one such feature has been identified, which results from an axial asymmetry of the ferromagnetic volume with respect to the *center of moment* of the uniformly magnetized diamagnetic (DM) sample. These artefacts have been studied in detail in [7] and are also discussed in the context of FM contaminations in [3]. To illustrate, let us consider a typical square diamagnetic sample with a FM point-like contamination in one of the edges. Let us also assume that for a given field $H_0$ within the measured range, the magnetization is zero, i.e., the FM and DM components have the same magnitude but opposite signal, thus canceling each other. If the sample is mounted such that the contaminated edge is at the top or the bottom, the FM and DM *centers of moment* are displaced from each other by about half of the sample length. Therefore, close to $H_0$, instead of a $V(z)$ shape as in figure 10, one measures a superposition of two dipoles with opposite sign and separated by a few millimeters in the $z$ direction. This produces an N-like shape, with a relative (absolute) maximum and a absolute (relative) minimum of comparable magnitude in the vicinity of $H_0$. This is always visible in the measured $V(z)$ data but can also affect the *M-H* (or similarly the *M-T*) curves as follows. Both *iterative* and *linear* fitting routines calculate the magnetic moment by mathematically fitting equation (1) to the measured response curve. The *linear* routine assumes a perfectly centered sample and therefore uses equation (1). For the *iterative* routine, $z$ is substituted by $(z - z_0)$ in equation (1), where the additional free parameter $z_0$ accounts for possible sample miscentering along the $z$-axis. When the latter is used, since it always assumes a $V(z)$ curve with one absolute extremum (figure 10), the best fit will be obtained for $z_0$ equal to the position of the largest of the two extrema. Close to $H_0$, this results in a large fitted offset with opposite signs below and above $H_0$ and a discontinuity of the measured magnetic moment. We note, however, that these symptoms can only be interpreted as an indication of an asymmetric distribution of the FM material with respect to the DM substrate which, in many cases but not necessarily, corresponds to the presence of contaminant material. Also, the absence of such effects can not be interpreted as evidence of absence of contamination. The distribution of the contaminant material projected onto the measurement axis may simply be symmetric enough to escape detection.

## 4. Conclusions

In summary, we have established the practical limits of SQUID magnetometry for the detection of ferromagnetism in nanomaterials deposited on diamagnetic substrates with comparable magnetic signal. We have shown that, when proper procedures are followed, extrinsic magnetic signals can be reproducibly kept below $5 \times 10^{-7}$ emu ($5 \times 10^{-10}$ Am$^2$). Although we have described such procedures, the reliability limits should be established independently for the sample processing and handling conditions specific to each experiment, by means of adequate and statistically relevant tests. We suggest that magnetic behaviour should only be reported reasonably above those limits, as we were unable to identify characteristics of the contaminant magnetism which could be generally used as criteria to distinguish it from intrinsic ferromagnetism.

## Acknowledgments

This work was supported by FCT Portugal (SFRH/BD/35761/2007, PTDC/FIS/098943/2008, PTDC/CTM-NAN/115125/2009), FWO Flanders, KULeuven projects GOA/2009/006 and INPAC EF/05/005 and the IUAP P6/42 program.

## References

[1] D W Abraham, M M Frank, and S Guha. *Appl. Phys. Lett.*, 87:252502, 2005.
[2] M. A. Garcia, E. Fernandez Pinel, J. de la Venta, A. Quesada, V. Bouzas, J. F. Fernandez, J. J. Romero, M. S. Martin Gonzalez, and J. L. Costa-Kramer. *J. Appl. Phys.*, 105:013925, 2009.
[3] A. Ney, T. Kammermeier, V. Ney, K. Ollefs, and S. Ye. *J. Magn. Magn. Mater.*, 320:3341–3346, 2008.
[4] D P Osterman and S J Williamson. *Rev. Sci. Instrum.*, 54:1380–1382, 1983.
[5] A Zieba. *Rev. Sci. Instrum.*, 64:3357–3375, 1993.
[6] L L Miller. *Rev. Sci. Instrum.*, 67:3201–3207, 1996.
[7] P Stamenov and J M D Coey. *Rev. Sci. Instrum.*, 77:015106, 2006.